Nonexponential spin decay in a quantum kinetic description of the D'yakonov-Perel' mechanism mediated by impurity scattering

M. Cosacchi, M. Cygorek, F. Ungar, and V. M. Axt
Theoretische Physik III, Universität Bayreuth, 95440 Bayreuth, Germany
(Received 14 February 2017; published 23 May 2017)

The electron spin dynamics in an optically excited narrow quantum well is studied, where the electron spins precess in a **k**-dependent magnetic field, while the electrons scatter at localized impurities. For the resulting spin decay, which is commonly known as the D'yakonov-Perel' mechansim, analytical expressions in the strong- and weak-scattering limits are available. It is found by the numerical solution of quantum kinetic equations in a broad range of parameters that, in situations that are typically relevant for ultrafast optical experiments, the dynamics of the total spin polarization significantly deviates from the pertinent analytical results. This is attributed to the broad spectral width of the optically excited spin-polarized electron distribution, which gives rise to a spin dephasing due to inhomogeneous broadening. Furthermore, it is found that the decay of the spin polarization need not be exponential. The notion of a spin decay time becomes ambiguous and different definitions of spin decay times can lead to different outcomes. The long-term dynamics of the decay of the spin polarization is even dominated by an algebraically decaying component. These findings highlight the importance of the effects of the broad spectral distribution of optically excited carriers in ultrashort magneto-optical experiments.

DOI: 10.1103/PhysRevB.95.195313

I. INTRODUCTION

In the field of spintronics [1–4], the spin dynamics in semiconductors has attracted a lot of interest in the last decades since the spin dephasing times in semiconductors can be orders of magnitude larger than, e.g., in metals [5,6]. There are two different approaches for studying the spin dynamics in semiconductors which have to be distinguished: transport [1,7–14] and optical experiments [15–20]. The former uses the fact that the injection of carriers into the semiconductor and the transmission from the semiconductor into another material can be strongly spin- dependent. Therefore, the resistivity of devices consisting of a semiconductor material between a spin injector and a spin filter is strongly affected by the dynamics of the carrier spins in the semiconductor [1,7], which paves the way for the development of spin transistors [7,21]. Optical experiments, on the other hand, allow a very direct control and readout of the carrier spins in a semiconductor structure via the spin selection rules and the magneto-optical Faraday and Kerr effect, e.g., in optical pump-probe measurements [16–20].

The literature on spin dynamics in semiconductors [22] typically lists the D'yakonov-Perel' (DP) [23], the Elliot-Yafet (EY) [24–26], and the Bir-Aronov-Pikus (BAP) [27] mechanisms as the main sources for the decay of a nonequilibrium carrier spin polarization. The BAP mechanism is due to the interaction between electron and hole spins and it is therefore mostly relevant for the electron spin dynamics in p-doped semiconductors [28]. Both the DP and the EY mechanisms originate from spin-orbit interaction (SOI) and the mixing of conduction and valence bands for nonzero wave vectors **k** according to $\mathbf{k}\cdot\mathbf{p}$ theory. The EY mechanism is based on the fact that, due to the band mixing for finite wave vectors **k**, the energy eigenstates of the quasifree carriers are no longer eigenstates of the spin operator. Thus scattering of electrons leading to a change of the wave vector **k** also leads to a change in the average electron spin. Another effect resulting from the mixing of valence and conduction bands is that a block-diagonalization, which eliminates the coupling of different bands renormalizes the crystal Hamiltonian, so that the conduction band block after block-diagonalization acquires an additional term that can be written in the form of a Zeeman energy with a **k**-dependent effective magnetic field. The DP mechanism describes the combined effect of the dephasing of electron spins caused by the precession in the strongly anisotropic **k**-dependent field and momentum scattering of the electrons at, e.g., impurities, other carriers or phonons. In the strong-scattering limit, D'yakonov and Perel' have derived [23] their well-known result that the spin decay rate is inversely proportional to the momentum scattering rate. Also in the weak-scattering limit, an analytical relation between spin decay and momentum scattering can be obtained [22,29]. However, there, the spin decay rate is proportional to the momentum scattering rate.

Another mechanism leading to a decay of the total electron spin polarization has been pointed out by Wu and Ning [30,31]: the spin precession frequency given by the magnitude of the effective field depends on the modulus $|\mathbf{k}|$ of the wave vector. Thus, when electrons with different kinetic energies take part in the spin dynamics, the presence of different precession frequencies gives rise to a dephasing of spins even in the absence of momentum scattering, where the conventional DP mechanism predicts no spin decay. This effect is referred to as inhomogeneous broadening by Wu *et al.* in Refs. [30,31] and is characterized by an algebraic spin decay $\propto\frac{1}{t}$ for long times [22]. In order to distinguish this mechanism from other effects typically associated with the term inhomogeneous broadening in the context of optical experiments on semiconductors, such as the linewidth broadening of excitons caused by spatial fluctuations of the environment [32], in the following, we use the term *dispersion-induced isotropic inhomogeneous broadening* (DIIB) for the spin dephasing induced by the $|\mathbf{k}|$ dependence of the effective magnetic field.

Numerous works in the literature have addressed the question of how the spin dynamics in semiconductors is affected by the DP, the EY, and the BAP mechanisms [22,33–41]. In particular, Wu *et al.* [22] have reviewed the contribution of

different spin dephasing and momentum scattering mechanisms to the total spin decay time using kinetic spin Bloch equations (KSBE). Most works focus on calculating spin transfer rates and their dependencies on certain parameters such as carrier concentration, temperature, external magnetic field, and so on [42,43]. However, rates are only well-defined if the spin decay is approximately exponential, which is *a priori* not clear. If the spin decay is nonexponential, the concept of a spin decay rate becomes ill-defined.

In this paper, we investigate the time evolution of the electron spin in an $Al_xGa_{1-x}As$ semiconductor quantum well (QW) after optical excitation with circularly polarized light. We consider the precession of electron spins in a **k**-dependent Dresselhaus or Rashba field and scattering of electrons at Al impurities. This is a situation which is conventionally described by the DP mechanism. Here, however, we use a microscopic quantum kinetic density matrix theory, which goes beyond the conventional DP picture in several aspects: first, by resolving the **k** space, we explicitly consider an ensemble of electrons, whereas the standard DP theory [23] describes a stochastic motion of a single electron. Thus our theory includes the spin dephasing due to DIIB [30,31]. Second, we do not *a priori* postulate the existence of a well-defined spin decay rate, i.e., we calculate the time evolution of the total electron spin explicitly and do not assume that it is exponential. This allows us to study the spin dynamics even when the notion of a spin decay rate is questionable. Finally, the quantum kinetic description goes beyond perturbation theory in the carrier-impurity interaction, the Markov approximation, and the single-particle picture as it includes explicitly correlations between carriers and impurities that are built up during the scattering. Our theory is applicable not only in the limiting cases of weak and strong scattering, but also in the intermediate regime and, therefore, allows us to study the range of validity of the results in the limiting cases.

We find that the time evolution of the total spin polarization after optical excitation can have different shapes, ranging between an exponentially damped oscillation to a Gaussian-like monotonic decay. There are also situations where the spin decays highly nonexponentially, has a minimum, and shows a slow decay at large times. Furthermore, the long-term dynamics can be dominated by an algebraic decay. In particular, we find that the broad width of the optically induced electron distribution has very important effects on the spin dynamics, highlighting the importance of DIIB for ultrafast optical experiments. Furthermore, we find that because of the nonexponential nature of the spin dynamics different definitions of a characteristic spin decay time can give quantitatively and qualitatively different results. This shows that the concept of a spin decay time has to be treated with care when discussing results of ultrafast optical experiments.

The paper is structured as follows: first, we set up a quantum kinetic theory for the dynamics of the electron density matrix as well as electron-impurity correlations. Subsequently, we derive the Markov limit of the quantum kinetic equations of motion and discuss theoretically certain known limiting cases. Then, we present numerical results of Markovian and quantum kinetic calculations for an optically excited $Al_xGa_{1-x}As$ quantum well with Dresselhaus and Rashba spin-orbit fields. Finally, we summarize the results.

II. THEORY

We study the spin dynamics in a semiconductor quantum well after optical excitation, which can be experimentally addressed by optical pump-probe measurements such as in time-resolved Kerr rotation experiments [20]. More specifically, we consider a D'yakonov-Perel'-type system [23] where the optically induced electron spins precess in a **k**-dependent effective magnetic field like the Dresselhaus [44] or Rashba [45] field and the carriers are subject to momentum scattering at localized impurities. Depending on the sample and the excitation conditions, there are also situations in which other momentum relaxation mechanisms are dominant, such as phonon scattering or carrier-carrier scattering [22,28].

Here, however, we consider a narrow $Al_xGa_{1-x}As$ quantum well with $Al_yGa_{1-y}As$ barriers, where $y > x$ to ensure the confinement of carriers in the well. We focus on a situation where the Al concentration x in the quantum well is not too small, the temperature of the sample is low enough to suppress phonon scattering and the intrinsic sample is excited with low or moderate intensity so that carrier-carrier interactions are of minor importance. Then, the momentum scattering at the Al impurities dominates and other momentum scattering mechanisms are negligible. Furthermore, we assume that the spins of the optically induced holes dephase fast due to the strong spin-orbit interaction in the valence band and we are only interested in the dynamics of the conduction band electron spins. Moreover, the quantum well is assumed to be narrow enough so that only the lowest confinement state has to be considered and the relevant electronic states can be described by plane waves with two-dimensional in-plane wave vectors **k**.

A. Hamiltonian

The Hamiltonian for conduction band electrons in a narrow $Al_xGa_{1-x}As$ quantum well is

$$\hat{H} = \hat{H}_0 + \hat{H}_{\mathrm{SO}} + \hat{H}_{\mathrm{Imp}}\,, \tag{1}$$

where

$$\hat{H}_0 = \sum_{\sigma\mathbf{k}} \hbar\omega_{\mathbf{k}} \hat{c}^\dagger_{\sigma\mathbf{k}} \hat{c}_{\sigma\mathbf{k}} \tag{2}$$

describes the spin-independent part of the band structure, which we assume to be parabolic according to $\omega_{\mathbf{k}} = \frac{\hbar\mathbf{k}^2}{2m^*}$ with the two-dimensional in-plane wave vector **k** and in-plane effective mass m^*. The symbol $\sigma \in \{\uparrow, \downarrow\}$ denotes the spin index and distinguishes the two conduction subbands. Finally, $\hat{c}^\dagger_{\sigma\mathbf{k}}$ and $\hat{c}_{\sigma\mathbf{k}}$ are the electron creation and annihilation operators, respectively.

The spin-orbit interaction (SOI) is described by the Hamiltonian

$$\hat{H}_{\mathrm{SO}} = \sum_{\sigma\sigma'\mathbf{k}} \hbar\boldsymbol{\Omega}_{\mathbf{k}} \cdot \mathbf{s}_{\sigma\sigma'} \hat{c}^\dagger_{\sigma\mathbf{k}} \hat{c}_{\sigma'\mathbf{k}}\,. \tag{3}$$

Here, $\mathbf{s}_{\sigma\sigma'} = \frac{1}{2}\boldsymbol{\sigma}_{\sigma\sigma'}$, where $\boldsymbol{\sigma}$ denotes the vector of Pauli matrices and $\boldsymbol{\Omega}_{\mathbf{k}}$ is the **k**-dependent effective magnetic field arising from bulk (BIA) or structure inversion asymmetries (SIA) that result in Dresselhaus [44] and Rashba [45] contributions to the

effective magnetic field of the form [46,47]

$$\mathbf{\Omega}_{\mathbf{k}_1} = \mathbf{\Omega}_{\mathbf{k}_1}^{\text{Rashba}} + \mathbf{\Omega}_{\mathbf{k}_1}^{\text{Dresselhaus}}, \tag{4a}$$

$$\mathbf{\Omega}_{\mathbf{k}_1}^{\text{Rashba}} = 2\frac{\alpha_R}{\hbar}\begin{pmatrix} k_y \\ -k_x \end{pmatrix}, \tag{4b}$$

$$\mathbf{\Omega}_{\mathbf{k}_1}^{\text{Dresselhaus}} = 2\frac{\beta_D}{\hbar}\begin{pmatrix} k_y \\ k_x \end{pmatrix}, \tag{4c}$$

for a (001)-grown quantum well with zinc-blende crystal structure. The spin-orbit interaction described by $\hat{H}_{\text{SO}}$ is responsible for a precession of the electron spins in the effective magnetic field.

The momentum scattering is induced by the interaction between carriers and localized Al impurities in the $Al_xGa_{1-x}As$ quantum well. In contrast to the case of charged impurities as discussed, e.g., in Ref. [30], Al ions are incorporated isoelectrically in the GaAs matrix. Since the long-range part of the Coulomb interaction between Al impurities and the quasi-free carriers is equally screened by the valence electrons as the long-range contribution of the interaction between the carriers and the Ga ions that are replaced by Al ions, the conduction band electrons experience only an effective short-range potential at unit cells with Al ions, which can be described by the Hamiltonian [48]

$$\hat{H}_{\text{Imp}} = J\sum_{Ii}\delta(\mathbf{r}_i - \mathbf{R}_I). \tag{5a}$$

The coupling constant is given by J, while $\mathbf{r}_i$ and $\mathbf{R}_I$ denote the electron and impurity positions, respectively. In second quantization, $\hat{H}_{\text{Imp}}$ reads

$$\hat{H}_{\text{Imp}} = \frac{J}{V}\sum_{I=1}^{N}\sum_{\sigma\mathbf{k}\mathbf{k}'} e^{-i(\mathbf{k}'-\mathbf{k})\cdot\mathbf{R}_I}\hat{c}^\dagger_{\sigma\mathbf{k}}\hat{c}_{\sigma\mathbf{k}'} \tag{5b}$$

with the system's volume V and the number of impurity atoms N. In the following, we assume that the impurity positions are determined by a fixed random distribution. This implies that the impurity system is not changed by $\hat{H}_{\text{Imp}}$ and the scattering is elastic. Thus $\hat{H}_{\text{Imp}}$ does not result in a thermalization as, e.g., momentum scattering due to carrier-phonon interactions.

We do not simulate the optical excitation of carriers via a light-matter interaction Hamiltonian explicitly. Instead, we assume that an ultrashort circularly polarized Gaussian pump pulse creates a spin polarized electron distribution at $t \approx 0$. The corresponding optically excited carrier distribution is then taken as an initial value for the differential equations of motion. The validity of such a treatment has been previously verified for similar situations encountered in studies of diluted magnetic semiconductors [49].

B. Equations of motion

We are interested in the spin dynamics of the conduction band electrons in an $Al_xGa_{1-x}As$ quantum well, which can be obtained directly from the reduced electron density matrix $\langle\hat{c}^\dagger_{\sigma_1\mathbf{k}_1}\hat{c}_{\sigma_2\mathbf{k}_1}\rangle$. Its time evolution is determined by the Heisenberg equation of motion for the operator $\hat{c}^\dagger_{\sigma_1\mathbf{k}_1}\hat{c}_{\sigma_2\mathbf{k}_1}$.

While the effective single-particle Hamiltonians $\hat{H}_0$ and $\hat{H}_{\text{SO}}$ alone would yield a closed set of equations of motion for the reduced single-particle density matrix, the carrier-impurity interaction $\hat{H}_{\text{Imp}}$ is responsible for a build-up of correlations between the electrons and impurities. This can be seen most clearly by considering the time evolution of the reduced density matrix due to the carrier-impurity interaction

$$-i\hbar\frac{\partial}{\partial t}\bigg|_{\hat{H}_{\text{Imp}}}\langle\hat{c}^\dagger_{\sigma_1\mathbf{k}_1}\hat{c}_{\sigma_2\mathbf{k}_1}\rangle = \langle[\hat{H}_{\text{Imp}},\hat{c}^\dagger_{\sigma_1\mathbf{k}_1}\hat{c}_{\sigma_2\mathbf{k}_1}]\rangle. \tag{6}$$

Calculating the commutator and taking the average over the result yields terms of the form

$$\langle e^{-i(\mathbf{k}_2-\mathbf{k}_1)\cdot\mathbf{R}_I}\hat{c}^\dagger_{\sigma_1\mathbf{k}_1}\hat{c}_{\sigma_2\mathbf{k}_2}\rangle, \tag{7}$$

which, in general, cannot be expressed in terms of the reduced density matrix alone since the averaging also involves taking an average over the random distribution of the positions $\mathbf{R}_I$ of the impurities. Only for $\mathbf{k}_2 = \mathbf{k}_1$, where $e^{-i(\mathbf{k}_2-\mathbf{k}_1)\cdot\mathbf{R}_I} \equiv 1$, the correlation in Eq. (7) reduces to $\langle\hat{c}^\dagger_{\sigma_1\mathbf{k}_1}\hat{c}_{\sigma_2\mathbf{k}_2}\rangle$. In the spirit of Kubo's cumulant expansion [50], we subtract the uncorrelated (mean-field) part of the term in Eq. (7) and define for $\mathbf{k}_2 \neq \mathbf{k}_1$ the cumulants or true correlations

$$\begin{aligned}&\delta\langle e^{-i(\mathbf{k}_2-\mathbf{k}_1)\cdot\mathbf{R}_I}\hat{c}^\dagger_{\sigma_1\mathbf{k}_1}\hat{c}_{\sigma_2\mathbf{k}_2}\rangle \\ &:= \langle e^{-i(\mathbf{k}_2-\mathbf{k}_1)\cdot\mathbf{R}_I}\hat{c}^\dagger_{\sigma_1\mathbf{k}_1}\hat{c}_{\sigma_2\mathbf{k}_2}\rangle - \langle e^{-i(\mathbf{k}_2-\mathbf{k}_1)\cdot\mathbf{R}_I}\rangle\langle\hat{c}^\dagger_{\sigma_1\mathbf{k}_1}\hat{c}_{\sigma_2\mathbf{k}_2}\rangle.\end{aligned} \tag{8}$$

Thus the reduced electron density matrix is driven by carrier-impurity correlations. Similarly, the equations of motion for the carrier-impurity correlations contain terms of the form

$$\langle e^{-i(\mathbf{k}-\mathbf{k}_2)\cdot\mathbf{R}_I}e^{-i(\mathbf{k}_2-\mathbf{k}_1)\cdot\mathbf{R}_{I'}}\hat{c}^\dagger_{\sigma_1\mathbf{k}_1}\hat{c}_{\sigma_2\mathbf{k}}\rangle. \tag{9}$$

For $I' = I$, $\mathbf{k} = \mathbf{k}_2$, or $\mathbf{k}_2 = \mathbf{k}_1$, this expression reduces to the carrier-impurity correlations defined in Eq. (7) or the carrier density matrix $\langle\hat{c}^\dagger_{\sigma_1\mathbf{k}_1}\hat{c}_{\sigma_2\mathbf{k}_1}\rangle$. In the remaining cases, the cumulant expansion [50] for three commuting random variables $A = e^{-i(\mathbf{k}-\mathbf{k}_2)\cdot\mathbf{R}_I}$, $B = e^{-i(\mathbf{k}_2-\mathbf{k}_1)\cdot\mathbf{R}_{I'}}$ and $C = \hat{c}^\dagger_{\sigma_1\mathbf{k}_1}\hat{c}_{\sigma_2\mathbf{k}}$ can be applied:

$$\begin{aligned}\langle ABC\rangle =& \delta\langle ABC\rangle + \langle A\rangle\delta\langle BC\rangle + \langle B\rangle\delta\langle AC\rangle \\ &+ \langle C\rangle\delta\langle AB\rangle + \langle A\rangle\langle B\rangle\langle C\rangle.\end{aligned} \tag{10}$$

Here, we neglect higher order correlations involving different impurity positions $\mathbf{R}_I$ and $\mathbf{R}_{I'}$, so that $\delta\langle ABC\rangle = \delta\langle AB\rangle = 0$. The remaining terms involve either $\langle A\rangle$ or $\langle B\rangle$. Assuming an on average homogeneous impurity distribution [51], one obtains

$$\langle e^{-i\mathbf{k}\cdot\mathbf{R}_I}\rangle = \delta_{\mathbf{k}0} \tag{11}$$

and therefore $\langle A\rangle = \delta_{\mathbf{k},\mathbf{k}_2}$ as well as $\langle B\rangle = \delta_{\mathbf{k}_2,\mathbf{k}_1}$. Thus all terms in Eq. (10) vanish, except for those with $\mathbf{k} = \mathbf{k}_2$ or $\mathbf{k}_2 = \mathbf{k}_1$, which can be expressed by the lowest-order cumulants defined in Eq. (8) and the carrier density matrix.

This way, a closed set of equations of motion is obtained for the dynamical variables

$$C^{\sigma_2}_{\sigma_1\mathbf{k}_1} := \langle\hat{c}^\dagger_{\sigma_1\mathbf{k}_1}\hat{c}_{\sigma_2\mathbf{k}_1}\rangle, \tag{12a}$$

$$\overline{C}^{\sigma_2\mathbf{k}_2}_{\sigma_1\mathbf{k}_1} := V\delta\langle e^{-i(\mathbf{k}_2-\mathbf{k}_1)\cdot\mathbf{R}_I}\hat{c}^\dagger_{\sigma_1\mathbf{k}_1}\hat{c}_{\sigma_2\mathbf{k}_2}\rangle, \tag{12b}$$

where $C^{\sigma_2}_{\sigma_1\mathbf{k}_1}$ is the electron density matrix and $\overline{C}^{\sigma_2\mathbf{k}_2}_{\sigma_1\mathbf{k}_1}$ are the carrier-impurity correlations, where the latter are only defined

for $\mathbf{k}_2 \neq \mathbf{k}_1$. It is convenient to rescale the correlations by the factor V so that they remain finite in the limit $V \to \infty$. Note that a similar correlation expansion has been developed and applied in Refs. [52–55], e.g., for investigations of the influence of interface roughness on exciton line shapes.

The quantum kinetic equations of motion for the dynamical variables are

$$-i\hbar\frac{\partial}{\partial t}C^{\sigma_2}_{\sigma_1\mathbf{k}_1} = \hbar\boldsymbol{\Omega}_{\mathbf{k}_1}\cdot\sum_{\sigma}\left(\mathbf{s}_{\sigma\sigma_1}C^{\sigma_2}_{\sigma\mathbf{k}_1} - \mathbf{s}_{\sigma_2\sigma}C^{\sigma}_{\sigma_1\mathbf{k}_1}\right) + \frac{JN}{V^2}\sum_{\mathbf{k}\neq\mathbf{k}_1}\left(\overline{C}^{\sigma_2\mathbf{k}_1}_{\sigma_1\mathbf{k}} - \overline{C}^{\sigma_2\mathbf{k}}_{\sigma_1\mathbf{k}_1}\right), \tag{13a}$$

$$\begin{aligned}-i\hbar\frac{\partial}{\partial t}\overline{C}^{\sigma_2\mathbf{k}_2}_{\sigma_1\mathbf{k}_1} &= \hbar\left(\omega_{\mathbf{k}_1} - \omega_{\mathbf{k}_2}\right)\overline{C}^{\sigma_2\mathbf{k}_2}_{\sigma_1\mathbf{k}_1} \\ &+ \sum_{\sigma}\hbar\left(\boldsymbol{\Omega}_{\mathbf{k}_1}\cdot\mathbf{s}_{\sigma\sigma_1}\overline{C}^{\sigma_2\mathbf{k}_2}_{\sigma\mathbf{k}_1} - \boldsymbol{\Omega}_{\mathbf{k}_2}\cdot\mathbf{s}_{\sigma_2\sigma}\overline{C}^{\sigma\mathbf{k}_2}_{\sigma_1\mathbf{k}_1}\right) \\ &+ \frac{J}{V}\left(\sum_{\mathbf{k}\neq\mathbf{k}_1}\overline{C}^{\sigma_2\mathbf{k}_2}_{\sigma_1\mathbf{k}} - \sum_{\mathbf{k}\neq\mathbf{k}_2}\overline{C}^{\sigma_2\mathbf{k}}_{\sigma_1\mathbf{k}_1}\right) \\ &+ J\left(C^{\sigma_2}_{\sigma_1\mathbf{k}_2} - C^{\sigma_2}_{\sigma_1\mathbf{k}_1}\right).\end{aligned} \tag{13b}$$

The first term on the right-hand side (r.h.s.) of Eq. (13a) describes the mean field precession of the electron spins in the effective field while the second term incorporates the changes of the electron density matrix due to the carrier-impurity correlations that mediate the impurity scattering. The equation of motion (13b) for the correlations has the structure of an oscillator with a frequency corresponding to the difference in kinetic energies $\hbar\omega_{\mathbf{k}_2} - \hbar\omega_{\mathbf{k}_1}$ (first term on the r.h.s.) driven by the electron density matrix $C^{\sigma_2}_{\sigma_1\mathbf{k}_1}$ via the last term on the r.h.s. of Eq. (13b). The second term describes the precession of the carrier-impurity correlations around the effective magnetic field and the third term accounts for changes of the wave vectors of the correlations caused by the carrier-impurity interaction.

C. Markov limit

The full quantum kinetic equations of motion (13) describe a dynamics of the electron density matrix that is non-Markovian in general, i.e., the correlations induce a finite memory. It is instructive to consider the Markovian limit of the quantum kinetic equations because of two reasons: On the one hand, to investigate the importance of finite-memory effects, and on the other hand, to derive an analytic expression for the momentum scattering rate, so that our theory can be related to more commonly used approximate descriptions of the DP mechanism.

The Markov limit of the quantum kinetic equations of motion is obtained by neglecting the second and third terms on the r.h.s. of Eq. (13b), which allows one to formally integrate the correlations yielding

$$\overline{C}^{\sigma_2\mathbf{k}_2}_{\sigma_1\mathbf{k}_1}(t) = e^{i(\omega_{\mathbf{k}_1}-\omega_{\mathbf{k}_2})t}\left[\overline{C}^{\sigma_2\mathbf{k}_2}_{\sigma_1\mathbf{k}_1}(t_0) + \int_{t_0}^{t}dt' i\frac{J}{\hbar} \times \left(C^{\sigma_2}_{\sigma_1\mathbf{k}_2}(t') - C^{\sigma_2}_{\sigma_1\mathbf{k}_1}(t')\right)e^{-i(\omega_{\mathbf{k}_1}-\omega_{\mathbf{k}_2})t'}\right]. \tag{14}$$

Neglecting the respective terms in the equation for the correlations can be justified as follows: the third term in Eq. (13b) is a higher order term with respect to the coupling constant. Furthermore, it consists of a sum of correlations with different wave vectors that oscillate with different frequencies and can therefore be expected to dephase fast. The second term in Eq. (13b) mainly accounts for the fact that the energy eigenvalues and eigenstates of the semiconductor crystal, which define the electronic states between which elastic momentum scattering events take place, are modified by the effective magnetic field. Here, however, we mainly consider situations where the spin-orbit splitting of the conduction subbands $\hbar\Omega_{\mathbf{k}}$ is on average smaller than the average kinetic energy and the modification of the band structure due to the effective field is of minor importance. Situations where this modification is important have been discussed in Ref. [56] on the level of a Markovian theory. Note that it is also possible to formally integrate Eq. (13b) accounting for the second term on the r.h.s., but the resulting Markovian equations become more involved [57]. An *a posteriori* justification for neglecting the respective terms in the equations of motion will be given by comparing numerical calculations of the full quantum kinetic equations and the Markovian equations.

The Markovian approximation is characterized by the assumption of a short memory, which implies that the density matrices $C^{\sigma_2}_{\sigma_1\mathbf{k}_1}(t')$ in Eq. (14) can be evaluated at $t' = t$ and the lower limit of the memory integral can be extended to $t_0 \to -\infty$ [58,59]. Finally, using $\int_{-\infty}^{0}dt\, e^{-i\Delta\omega t} = \pi\delta(\Delta\omega) + \mathcal{P}\frac{i}{\Delta\omega}$ and assuming that the correlations are initially zero $\overline{C}^{\sigma_2\mathbf{k}_2}_{\sigma_1\mathbf{k}_1}(t_0 \to -\infty) = 0$, we obtain

$$-i\hbar\frac{\partial}{\partial t}C^{\sigma_2}_{\sigma_1\mathbf{k}_1} = \hbar\boldsymbol{\Omega}_{\mathbf{k}_1}\cdot\sum_{\sigma}\left(\mathbf{s}_{\sigma\sigma_1}C^{\sigma_2}_{\sigma\mathbf{k}_1} - \mathbf{s}_{\sigma_2\sigma}C^{\sigma}_{\sigma_1\mathbf{k}_1}\right) + 2\pi i\frac{J^2N}{V^2}\sum_{\mathbf{k}\neq\mathbf{k}_1}\left(C^{\sigma_2}_{\sigma_1\mathbf{k}_1} - C^{\sigma_2}_{\sigma_1\mathbf{k}}\right)\delta\left(\hbar\omega_{\mathbf{k}} - \hbar\omega_{\mathbf{k}_1}\right). \tag{15}$$

The contributions from the principal value cancel exactly. Equation (15) can be rewritten in the quasi-continuous limit $\sum_{\mathbf{k}} \to \int d(\hbar\omega_{\mathbf{k}})D^{2D}(\hbar\omega_{\mathbf{k}})$ with the two-dimensional spectral density of states $D^{2D}(\hbar\omega) = \frac{Am^*}{2\pi\hbar^2}$ in terms of the more intuitive variable $\langle\mathbf{s}_{\mathbf{k}_1}\rangle = \sum_{\sigma\sigma'}\mathbf{s}_{\sigma\sigma'}C^{\sigma'}_{\sigma\mathbf{k}_1}$, i.e., the average spin in the electronic states with wave vector $\mathbf{k}_1$. We obtain

$$\frac{\partial}{\partial t}\langle\mathbf{s}_{\mathbf{k}_1}\rangle = \boldsymbol{\Omega}_{\mathbf{k}_1}\times\langle\mathbf{s}_{\mathbf{k}_1}\rangle - \frac{1}{\tau_p}\left(\langle\mathbf{s}_{\mathbf{k}_1}\rangle - \langle\bar{\mathbf{s}}_{k_1}\rangle\right), \tag{16}$$

with the momentum scattering rate

$$\frac{1}{\tau_p} = \frac{4J^2m^*x}{\hbar^3da^3}, \tag{17}$$

where x denotes the impurity concentration, d the thickness of the quantum well, and a the lattice constant of the crystal. The average spin in the shell of states with modulus k_1 of the wave vector $\mathbf{k}_1$ is given by

$$\langle\bar{\mathbf{s}}_{k_1}\rangle = \frac{1}{2\pi}\int_0^{2\pi}d\varphi\,\langle\mathbf{s}_{\mathbf{k}(k_1,\varphi)}\rangle, \tag{18}$$

where

$$\mathbf{k}(k_1,\varphi) = \begin{pmatrix} k_1\cos(\varphi) \\ k_1\sin(\varphi) \end{pmatrix}. \tag{19}$$

Thus, in the Markov limit, the time evolution of the electron spins is given by a precession of the spin in the **k**-dependent magnetic field and a redistribution of electron spins within a shell of fixed kinetic energy $\hbar\omega_{\mathbf{k}_1}$ with the momentum scattering rate τ_p^{-1}. Note that the Markovian equation of motion (16) can also be derived by other approaches [29] and they are, in fact, also applicable in settings where a phenomenological momentum scattering rate is used to incorporates additional effects due to, e.g., carrier-carrier or carrier-phonon scattering. Thus the results obtained from the Markovian equations are valid in more general DP scenarios where the momentum scattering does not need to be caused by localized impurities.

D. Limiting cases

Equations (13) and (16) describe the time evolution of an ensemble of optically induced electron spins. In contrast, the conventional description of the DP mechanism, which can be used to derive analytic expressions for the spin relaxation time in limiting cases, is based on a different picture where a single electron is considered which performs a stochastic motion in **k** space [22,23,60]. Here, we review the basic results of this stochastic picture.

In the conventional DP picture, it is assumed that the electron's wave vector **k** changes randomly after a time interval corresponding to a correlation time τ_c, which we identify with the momentum scattering time τ_p defined in Eq. (17). During this correlation time, the electron spin precesses about the effective field $\mathbf{\Omega}_{\mathbf{k}}$. Thus between each scattering event the electron spin changes about an angle of $\theta_{\mathbf{k}} = \tau_c\Omega_{\mathbf{k}}$. If the angle $\theta_{\mathbf{k}}$ is small, which implies that the scattering rate τ_c^{-1} is much larger than the typical precession frequency, the time evolution of the electron spin can be regarded as a random walk consisting of $n = t/\tau_c$ time steps. The root mean square of the precession angle is then given by

$$\sqrt{\Delta\theta^2} = \sqrt{\langle\theta_{\mathbf{k}}^2\rangle\frac{t}{\tau_c}} = \sqrt{\langle\Omega_{\mathbf{k}}^2\rangle\tau_c t}, \tag{20}$$

which is of the order of unity at the spin relaxation time

$$\tau_s \sim \frac{1}{\langle\Omega_{\mathbf{k}}^2\rangle\tau_c}, \tag{21}$$

where the brackets indicate the average over the **k**-space states available for the random walk process. This way, one obtains the well-known DP result that the spin relaxation time is predicted to be inversely proportional to the momentum relaxation time.

As stated above, the derivation of the expression for the spin relaxation time τ_s in Eq. (21) requires the assumption of the strong scattering limit $\tau_c^{-1} \gg \sqrt{\langle\Omega_{\mathbf{k}}^2\rangle}$. However, analytic expressions for the spin relaxation time can also be obtained in the opposite limit, $\tau_c^{-1} \ll \sqrt{\langle\Omega_{\mathbf{k}}^2\rangle}$ [29]. This can be done by starting from Eq. (16) and considering an initial carrier spin polarization along the z axis (growth direction). First, the z component of Eq. (16) is differentiated. In the resulting equation, the expressions $\langle s_{\mathbf{k}_1}^x\rangle$ and $\langle s_{\mathbf{k}_1}^y\rangle$ have to be eliminated by expressing them in terms of $\langle s_{\mathbf{k}_1}^z\rangle$ and $\frac{\partial}{\partial t}\langle s_{\mathbf{k}_1}^z\rangle$ using again Eq. (16). If terms higher than first order in the momentum scattering rate τ_p^{-1} are neglected and if it is assumed that the modulus of the precession frequency is independent of the polar angle of $\mathbf{k}_1$, i.e., one can write $\sqrt{\mathbf{\Omega}_{\mathbf{k}_1}^2} = \Omega_{k_1}$, one obtains the second-order differential equation for the z component of the average electron spin:

$$\frac{\partial^2}{\partial t^2}\langle\bar{s}_{k_1}^z\rangle + \frac{1}{\tau_p}\frac{\partial}{\partial t}\langle\bar{s}_{k_1}^z\rangle + \Omega_{k_1}^2\langle\bar{s}_{k_1}^z\rangle = 0. \tag{22}$$

Equation (22) has the form of a damped oscillator whose solution for $\frac{1}{\tau_p} \ll \Omega_{k_1}$ is an oscillation with frequency Ω_{k_1} that decays exponentially with the relaxation rate

$$\frac{1}{\tau_s} = \frac{1}{2\tau_p}. \tag{23}$$

Thus Eq. (23) predicts that, in the weak-scattering limit, the spin relaxation rate is proportional to the momentum relaxation rate.

It is noteworthy that, in contrast to the strong-scattering limit, the weak-scattering limit supports oscillations of the spin polarization. Thus, when an ensemble of electrons with different precession frequencies is considered, the superposition of the different oscillations may additionally lead to a dephasing, which causes a decay of the total electron spin even in the absence of momentum scattering $\tau_p^{-1} = 0$. This effect has been described by Ning *et al.* as an inhomogeneous broadening mechanism and was explored numerically in Refs. [30,31].

In situations where the electron occupation is well described by a quasi-equilibrium Fermi distribution with a significant Fermi energy, such as in n-doped systems or in transport experiments, only electronic states with a wave vector close to the Fermi wave vector $|\mathbf{k}| \approx k_F$ are relevant for the spin dynamics. Because the modulus $|\mathbf{k}|$ of the wave vector **k** determines the precession frequency $|\mathbf{\Omega}_{\mathbf{k}}|$, there is essentially only one precession frequency present in these situations and no DIIB takes place.

In contrast, in the case of an optically induced spin-polarized electron distribution in an intrinsic semiconductor, the spectral width of the exciting laser, e.g., due to the energy-time uncertainty associated with the finite duration of the laser pulse, gives rise to a corresponding finite spectral width of the electron distribution. In general, this translates into a non-negligible width of the distribution of the modulus $|\mathbf{k}|$ of the wave vectors of spin polarized carriers. Therefore, here, the DIIB can be expected to be relevant [61].

The qualitative shape of the time evolution of the total electron spin due to the DIIB alone, i.e., in the absence of momentum scattering $\tau_p \to \infty$, can be discussed in some limiting cases. First, consider the case of the initial distribution of spin polarized electrons defined by

$$n_{\mathbf{k}}(t=0) = \begin{cases} n_0, |\mathbf{k}| \in \left[k_0 - \frac{1}{2}\Delta k; k_0 + \frac{1}{2}\Delta k\right] \\ 0, \text{ else} \end{cases}, \tag{24a}$$

$$s_{\mathbf{k}}^z(t=0) = \tfrac{1}{2}n_{\mathbf{k}}(t=0), \tag{24b}$$

i.e., a distribution centered at k_0 with width Δk. Additionally, assume for simplicity that the system is only subject to Rashba spin-orbit interaction, so that

$$s^z_{\mathbf{k}}(t) \approx \frac{n_0}{2} \cos\left(2\frac{\alpha_R}{\hbar}kt\right). \tag{24c}$$

If $\Delta k \ll k_0$, we can assume that the two-dimensional k-dependent density of states is approximately constant $D^{2D}(k) \approx D^{2D}(k_0)$ and that the spin decay rate is essentially independent of $\mathbf{k}$. Then, the total spin is given by

$$\begin{aligned}
&\int dk\, D^{2D}(k) s^z_{\mathbf{k}}(t) \\
&\quad\approx \frac{n_0}{2} D^{2D}(k_0) \int_{k_0-\frac{1}{2}\Delta k}^{k_0+\frac{1}{2}\Delta k} dk\, \cos\left(2\frac{\alpha_R}{\hbar}kt\right) \\
&\quad= \frac{n_0}{2} D^{2D}(k_0) \frac{\sin\left[\frac{2\alpha_R(k_0+\frac{1}{2}\Delta k)t}{\hbar}\right] - \sin\left[\frac{2\alpha_R(k_0-\frac{1}{2}\Delta k)t}{\hbar}\right]}{2\frac{\alpha_R}{\hbar}t}.
\end{aligned} \tag{24d}$$

Thus, in this situation, we find that the total electron spin decays algebraically as $\frac{1}{t}$. Note that, because this behavior deviates strongly from an exponential decay, it is not possible to unambiguously associate a spin decay time with the spin dynamics.

In Ref. [61], another limiting case of the DIIB was discussed where a Gaussian initial spin-polarized spectral electron distribution was considered. It was found that, when the Gaussian distribution is centered around the band edge, i.e., $k \approx 0$, the time evolution of the total electron spin is given by an expression that resembles a one-sided Fourier-transform of a function with a Gaussian-like shape. Thus, the time evolution of the total electron spin itself is expected to be well approximated by a Gaussian rather than an exponential. This expectation was supported by numerical calculations in Ref. [61].

To summarize, in the Markov limit, an explicit expression for the spin relaxation rate τ_s^{-1} can be given in the strong-scattering limit $\tau_p^{-1} \gg \sqrt{\langle\Omega^2_{\mathbf{k}}\rangle}$ by Eq. (21), which is the original result of D'yakonov and Perel' and which predicts a spin relaxation rate inversely proportional to the momentum scattering rate. In the weak-scattering limit $\tau_p^{-1} \ll \sqrt{\langle\Omega^2_{\mathbf{k}}\rangle}$, the total spin in a single shell of states with fixed wave vector modulus $|\mathbf{k}|$ decays exponentially, where the spin relaxation rate is one half of the momentum relaxation rate. If, however, a distribution of spin-polarized electrons with varying values of $|\mathbf{k}|$ is optically excited, the DIIB mechanism predicts an algebraic or a Gaussian decay of the initial electron spin, depending on the spectral properties of the initial electron distribution.

III. RESULTS

Before presenting the results of numerical calculations, we first discuss the parameters used in our study as well as the details of the numerical methods used for the calculations.

A. System parameters

In this paper, we study the spin dynamics in a narrow $Al_xGa_{1-x}As$ quantum well immediately after optical excitation with circularly polarized light. The Al content x in the quantum well determines the momentum scattering and will be varied from zero to a few percent. Furthermore, we assume that the crystal can be well described by a zinc-blende lattice with parameters close to that of GaAs. For our calculations, we use the lattice constant $a = 565.35$ pm and the effective conduction band electron mass $m^* = 0.0665 \times m_0$, where m_0 is the free electron mass.

The coupling constant J is chosen in such a way [48] that it is, on a mean-field level, consistent with the conduction band offset at a $GaAs/Al_xGa_{1-x}As$ interface of $\Delta E_c = x \cdot 0.87$ eV in magnitude [62]. From this consideration, we obtain the coupling constant $J = \frac{a^3}{4}\Delta E_c = 39$ meV nm^3.

We choose the width of the quantum well to be $d = 10$ nm and only consider the lowest confinement state, for which $\langle k_z^2\rangle = (\pi/d)^2$. Then, the Dresselhaus parameter is given by $\beta_D = -\gamma\langle k_z^2\rangle$ with $\gamma = -11$ meVnm^3 (cf. Ref. [47]) yielding $\beta_D \approx 1$ meVnm.

The Rashba coefficient on the other hand is not only dependent on the material, but also on external electric fields and potentials [47]. We regard the Rashba coefficient as a tunable parameter and, for the sake of simplicity, set it to $\alpha_R = 0$, if not mentioned otherwise.

The optical driving is modeled by choosing suitable initial values for the electron density matrix. We imagine that a single circularly polarized Gaussian ultrafast femtosecond laser pulse has selectively excited spin-up electrons at $t = 0$ via the spin selection rules. Consistent with the spectral properties of such a pump pulse, we assume that at $t = 0$ only the spin-up occupations in the electron density matrix are populated and the spectral electron density is described by a Gaussian centered at an energy E_c above the band edge with a spectral standard deviation E_s.

B. Numerical methods

With the initial values described above, we numerically solve either the full quantum kinetic equation (13) or the Markovian equation (16) using a fourth-order Runge-Kutta algorithm. In order to arrive at a numerically tractable problem, we only consider electronic states up to a cutoff energy of about 20 meV. Furthermore, we take the quasi-continuous limit and replace sums over $\mathbf{k}$ with the corresponding two-dimensional $\mathbf{k}$-space integral, which is then treated in polar coordinates. The quantities depending on the polar angle of a wave vector are then expanded in terms of a discrete Fourier-series, which turns out to drastically speed up the calculations. This procedure makes it possible to equally treat all directions in $\mathbf{k}$ space, whereas in other approaches [30] only selected directions, e.g., the coordinate axes, could be resolved. The modulus $|\mathbf{k}|$ of the wave vector is discretized straightforwardly. It has been checked that neither refining the discretization of the $\mathbf{k}$ space and the time discretization nor increasing the cut-off energy further leads to visibly different results from those presented below.

C. Time evolution

We now discuss the general features of the time evolution of the electron spin polarization as shown in Fig. 1(a), where the spin polarization is defined by $\sum_{\mathbf{k}}\langle s^z_{\mathbf{k}}\rangle/(\frac{1}{2}N_e)$ with total

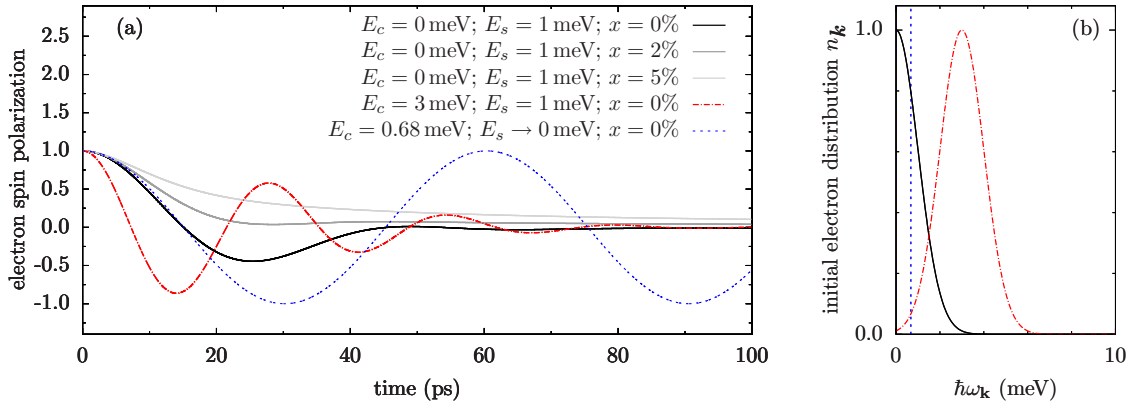

FIG. 1. (a) Time evolution of the optically induced electron spin calculated using the Markovian equation (16) for different impurity concentrations x and different initial electron distributions (Gaussian with central energy E_c above the band edge and standard deviation E_s) shown in (b).

electron number $N_e = \sum_{\mathbf{k}\sigma} C^{\sigma}_{\sigma\mathbf{k}}$. First of all, for low impurity concentrations and therefore low momentum scattering rates, pronounced oscillations of the total electron spin are found, whereas with increasing impurity concentration, the oscillations are suppressed and the electron spin polarization eventually decays monotonically. It can be seen from the results presented in Fig. 1(a) that the time evolution of the spin polarization is, in general, not well described by an exponentially damped oscillation, in particular for strong momentum scattering. For example, the graph for $x = 2\%$ shows nonmonotonic behavior whilst displaying always positive spin polarization. In contrast, negative spin polarizations would be expected from an exponentially damped cosine. It is noteworthy that the spin polarization decays even for $x = 0$, where, according to the stochastic picture without DIIB, the spin decay rate is expected to vanish, because $\tau_s^{-1} \approx \frac{1}{2}\tau_p^{-1} \to 0$.

In Fig. 1(a), also the spin dynamics for different initial electron distributions, which are shown in Fig. 1(b), is presented, corresponding to different properties of the exciting laser pulse. The center of the Gaussian E_c measured from the band edge can be controlled by the central frequency of the exciting laser and the width (standard deviation E_s) is related to the spectral properties of the laser pulse and has a lower bound due to the energy-time uncertainty. Nevertheless, it is instructive to discuss the theoretical case of a spectrally sharp initial spin-polarized carrier distribution with $E_s \to 0$, since this situation corresponds to turning off the effect of DIIB. The calculated time evolution in such a situation is depicted by the dotted line in Fig. 1(a). The center of the spectrally sharp initial electron distribution is chosen in such a way that it has the same average wave vector modulus $\langle|\mathbf{k}|\rangle$ as the initial electron distribution of the Gaussian with $E_c = 0$ meV and $E_s = 1$ meV. Comparing the corresponding calculations with zero and finite width of the electron distributions reveals that the DIIB is responsible for the spin decay in the absence of momentum scattering when the initial electron distribution has a finite width, whereas the oscillations continue indefinitely in calculations with spectrally sharp initial electron distribution if $x = 0$.

When the center of the electron distribution is shifted to higher energies (dashed-dotted line in Fig. 1), the oscillation frequency is also increased. This can be explained by the fact that the strength of the Rashba field $\Omega_{\mathbf{k}}$, which determines the typical precession frequency in the system, increases with increasing wave vector modulus $|\mathbf{k}|$ or, equivalently, increasing kinetic energy $\hbar\omega_{\mathbf{k}}$. Furthermore, the shift of the center of the electron distributions to higher energies leads to a reduction of the spin decay. We attribute this to the fact that for a Gaussian distribution with $E_c \gg E_s$, the situation resembles that of a spectrally sharp distribution and DIIB becomes less important.

D. Dependence of the spin relaxation times on momentum scattering

It is common in the literature [22,23,29] to discuss spin relaxation times or rates and their dependencies on different parameters. However, as we have seen in Fig. 1(a), the spin dynamics can strongly deviate from an exponential behavior that is implied by the concept of a spin relaxation rate. Thus the spin relaxation rate becomes ill-defined and ambiguous in certain cases.

Nevertheless, it is useful for understanding the qualitative dependence of the spin dynamics on the model parameters to consider quantities that can, to a certain extent, be interpreted as a characteristic time for the decay of the spin polarization. Here, we discuss two different definitions of spin decay times.

First, we fit a stretched exponential of the form

$$f(t) = \cos(\omega^f t)\exp\left[-\left(t/\tau_s^f\right)^n\right] \tag{25}$$

to the time evolution of the spin polarization, where ω^f, τ_s^f, and n are free parameters. The value of τ_s^f is then considered to be a measure of the spin decay time. The variable parameter n in the stretched exponential allows one to extract a meaningful spin decay time, e.g., in the limiting cases where an exponential or a Gaussian decay is expected. Second, we define τ_s^e to be the time after which the spin polarization has decreased to a value of $\frac{1}{e}$ of its initial value.

The parameters τ_s^e and τ_s^f are, in general, not equivalent. For example, τ_s^e is, in general, smaller than τ_s^f since also the oscillatory part $\cos(\omega^f t)$ leads to a decay of the total signal for small times. The different aspects of the spin dynamics measured by τ_s^e and τ_s^f can be discussed, e.g.,

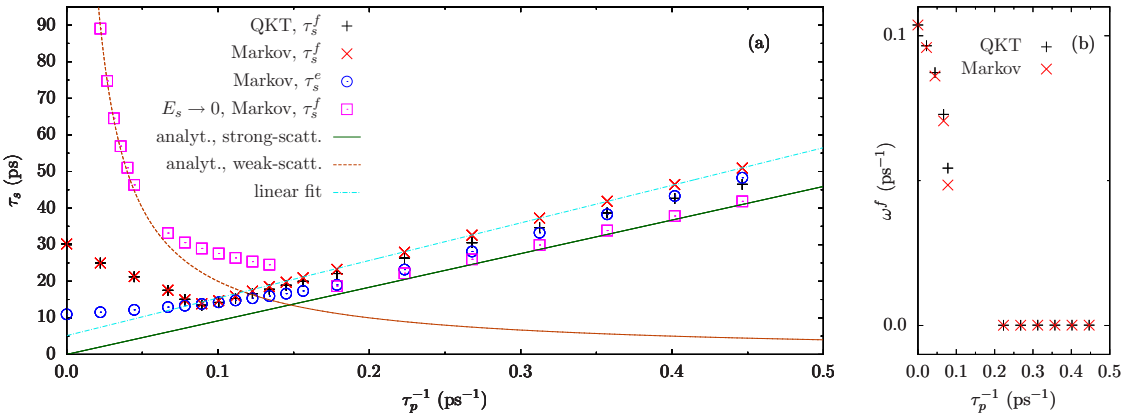

FIG. 2. (a) Spin decay time τ_s as a function of the momentum scattering rate τ_p^{-1}. The spin decay times are determined either by fitting a stretched exponential to the time evolution of the total spin polarization (τ_s^f) or by extracting the time after which the spin polarization is decayed to $\frac{1}{e}$ of its initial value (τ_s^e). The black pluses represent the results of calculations using the full quantum kinetic equations, while the remaining results are based on the Markovian equations of motion. The initial electron distributions used for the calculations are Gaussians with standard deviation $E_s = 1$ meV ($E_s \to 0$ for the results depicted as purple squares) centered at $E_c = 0$ meV [cf. Fig. 1(b)]. The analytic expressions in the strong- and weak-scattering limits are depicted as lines. For comparison, a linear fit through the last five points of the Markovian calculation of τ_s^f is shown. (b) Precession frequency of the total spin polarization obtained from the fitting procedure.

for the time evolution of the spin polarization for $x = 2\%$ in Fig. 1(a). There, the spin polarization first decays rapidly, then it increases again slightly and eventually decays very slowly toward zero. In this situation, the initial fast decay is measured by τ_s^e, while the slow decay at long times enters via the fit procedure in τ_s^f, which therefore measures the overall time scale of the spin decay.

In Fig. 2(a), the spin relaxation times τ_s^e and τ_s^f obtained from calculations of the spin dynamics are depicted as a function of the momentum scattering rate τ_p^{-1} determined from Eq. (17), which is varied by changing the impurity concentration x in the calculations. For comparison, the analytic results in the strong-scattering (solid straight line) and the weak-scattering (dashed hyperbola) limits are also depicted. It is found that above $\tau_p^{-1} \approx 0.1$ ps^{-1} both definitions of the spin decay times τ_s^f and τ_s^e lead to quantitatively different results, but depend qualitatively on the momentum scattering in a similar way and follow the general trend expected in the strong scattering limit. However, the numerically obtained spin decay times are consistently larger than the DP result, even for the largest studied momentum scattering rate. This tendency is visualized by fitting a line through the last five points of the Markovian result for τ_s^f.

Let us first concentrate on the Markovian results. For momentum scattering rates below 0.1 ps^{-1}, the results of τ_s^e and τ_s^f differ significantly: The spin decay time τ_s^e, which measures the fast initial decay, decreases monotonically with decreasing momentum scattering rate. However, τ_s^f, which measures the overall decay of the spin polarization including the long-time parts, shows a pronounced kink and a minimum at $\tau_p^{-1} \approx 0.1$ ps^{-1}. The discrepancy between τ_s^e and τ_s^f can be traced back to the fact that, for small momentum scattering rates, the time evolution of the spin oscillates and, as explained above, the oscillatory part leads to a decay of the spin that is included in the decay time τ_s^e but not in τ_s^f. The momentum-scattering-dependence of the precession frequency ω^f obtained by the fitting procedure is presented in Fig. 2(b) and supports this explanation. The results depicted in Fig. 2(b) indicate a bifurcation point close to the kink in τ_s^f in Fig. 2(a), below which oscillations occur. However, for values close to $\tau_p^{-1} = 0.1$ ps^{-1}, i.e., the region of the kink and the onset of the oscillations, the fitting procedure does not produce reliable results for ω^f, as small changes in the initial values of the fitting parameters can lead to significantly different results. Thus, in Fig. 2(b), we present only values for ω^f which are stable with respect to changes in the initial values of the fit parameters, which excludes the region of the expected bifurcation point.

It is noteworthy that the numerical results for the spin decay times for $\tau_p^{-1} \to 0$ disagree quantitatively and qualitatively with the analytical result $\tau_s = 2\tau_p$. In particular, the numerically obtained spin decay time τ_s^f increases approximately linearly to a finite value when $\tau_p^{-1} \to 0$, whereas the analytical result predicts a divergence, i.e., the spin decay time becomes infinitely long. However, as discussed in Sec. II D, DIIB can become important in the limit $\tau_p^{-1} \to 0$. To investigate the influence of DIIB, we present in Fig. 2(a) (purple squares) also the spin decay time τ_s^f obtained from calculations with a spectrally sharp initial electron distribution with the same value of $\langle|\mathbf{k}|\rangle$ as the Gaussian distribution used for the calculations discussed so far. It can be seen that the results of these simulations coincide with the analytical results in the strong- and weak-scattering limits.

Thus the discrepancies between numerical calculations for the Gaussian electron distribution and the analytical results in the respective limits can be traced back to the finite width of the spectral electron distribution. In the weak-scattering limit, the DIIB becomes important and dominates the spin decay. In the strong-scattering limit, the finite spectral width is found to increase the spin decay time, i.e., the spin decay is reduced. The reason for this is that the spin decay time according to the DP result given by Eq. (21) is inversely proportional to $\langle\Omega_{\mathbf{k}_1}^2\rangle$ and the spin relaxes faster in states with larger wave

vectors. Because of the finite width of the electron distribution, the ensemble of electron spins has parts whose spin relaxation is faster than the average and parts where it is slower. At medium and long times, the faster relaxing electron spins are already decayed, whereas the slower decaying electron spins remain and dominate the long-time dynamics. This effectively increases the decay time of the total spin polarization compared to the situation where only one precession frequency is present.

E. Influence of the central frequency of the exciting laser

In Fig. 2, we have studied a situation where a circularly polarized laser with central frequency matching the band gap was used for the optical excitation. Now, we consider an excitation with a central frequency larger than the band gap and discuss the influence of the energy difference between the laser and the band gap on the momentum-scattering-dependence of the spin decay time. To this end, we repeat the above Markovian calculations of the spin decay time τ_s^f with different values of the center E_c of the Gaussian initial spectral electron distribution and extract the fitted spin decay rate τ_s^f. The results are shown in Fig. 3 together with the analytical results in the strong- and weak-scattering limits.

It can be clearly seen that with increasing E_c the numerical and analytical results agree more and more. This can be explained by the fact that, when the center of the peak of the electron distribution E_c is increased while its width E_s remains constant, the ratio E_s/E_c decreases and the electron distribution effectively becomes spectrally sharp.

F. Rashba and Dresselhaus fields

The calculations presented so far only considered the Dresselhaus term as the origin of a **k**-dependent effective magnetic field. The effects of the Rashba interaction on the spin dynamics is shown in Fig. 4 for an optically excited quantum well without momentum scattering. It can be seen that the calculations using only the Dresselhaus field ($\alpha_R = 0$, $\beta_D = 1$ meVnm) and using only the Rashba interaction ($\alpha_R = 1$ meVnm, $\beta_D = 0$) yield identical results. In contrast, when both, the Rashba and the Dresselhaus terms are taken into account ($\alpha_R = \beta_D = 0.5$ meVnm), the spin polarization is found to decay much faster.

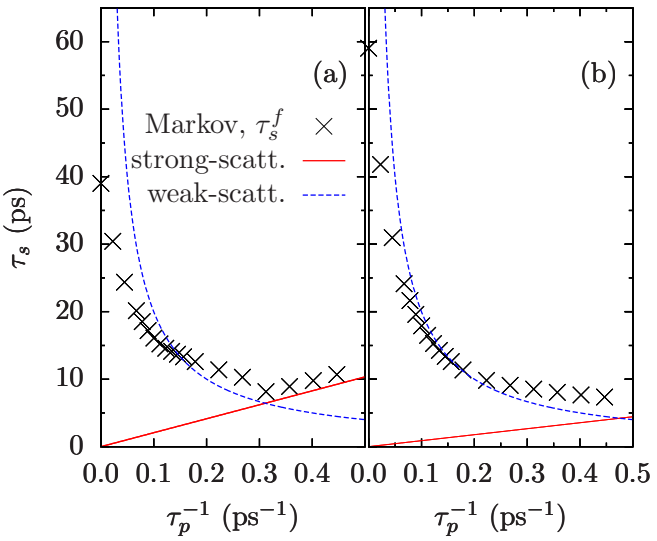

FIG. 3. Spin decay time τ_s^f as a function of the momentum scattering rate τ_p^{-1} for Gaussian initial electron distributions centered at (a) $E_c = 3$ and (b) 7 meV above the band edge and with standard deviation $E_s = 1$ meV.

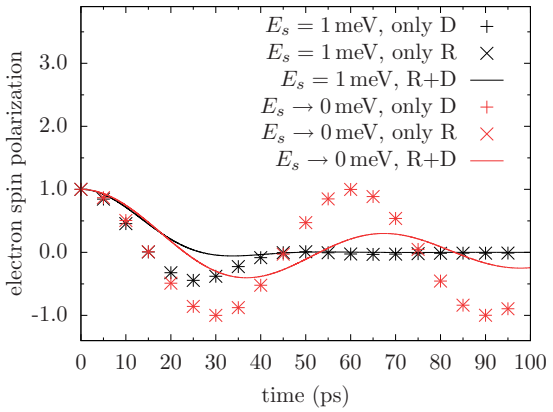

FIG. 4. Spin dynamics in a quantum well without momentum scattering ($x = 0$) subject to Dresselhaus (D), Rashba (R), or both (R+D) fields. The initial electron distribution is chosen to be a Gaussian centered at $E_c = 0$ with standard deviation $E_s = 1$ meV and $E_s \to 0$, respectively.

Even for calculations assuming a spectrally sharp initial electron distribution, the joint action of the Rashba and Dresselhaus field results in a significant decay of the spin polarization, whereas if the Rashba and Dresselhaus fields act alone an undamped oscillation is found. The reason for this is that, if only the Rashba or the Dresselhaus field is considered, the magnitude of the precession frequency is fixed by the wave vector modulus $|\mathbf{k}|$. When both interactions are present, this is not the case anymore and the magnitude of the precession frequency depends on the polar angle of the wave vector. Similar results for spectrally sharp distributions have been obtained in previous works based on rate equations [63,64]. In contrast, for distributions with finite spectral width typical in optical experiments the DIIB becomes important. As shown in Fig. 4, the DIIB strongly suppresses the spin coherence for all spin-orbit fields considered here. The fact that the impact of DIIB on the spin dynamics is similar for Rashba and Dresselhaus spin-orbit fields indicates that the qualitative trends obtained earlier in this work for the Dresselhaus field also apply for **k**-dependent fields of different origin.

G. Algebraic decay

In Fig. 5, the spin dynamics is shown on a double-logarithmic scale for a calculation with $x = 1.5\%$ and $E_s = 1$ meV accounting only for the Dresselhaus field. This scale allows us to discuss the qualitative behavior of the spin dynamics on long time scales. It can be clearly seen that the spin dynamic obeys an algebraic decay $\propto \frac{1}{t}$ rather than an exponential decay at times $\gtrsim$100 ps. Note that the divergence is only an artifact of negative spin polarizations displayed in a log-log plot.

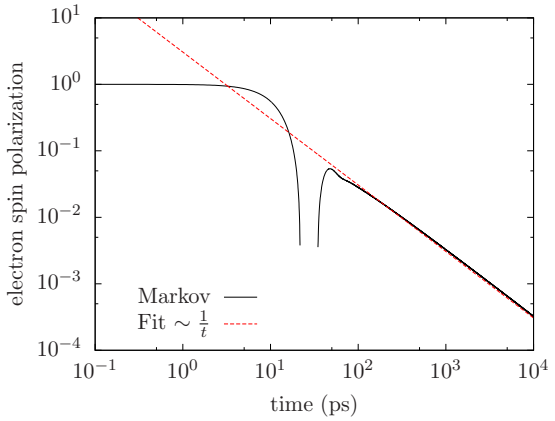

FIG. 5. Double-logarithmic plot of the long-time behavior of the spin dynamics calculated using the parameters $E_c = 0$, $E_s = 1$ meV, $\alpha_R = 0$, $\beta_D = 1$ meV nm, and $x = 1.5\%$.

As discussed in Sec. II D, an algebraic decay is a result of an averaging over undamped oscillatory components with a variation in the distribution of oscillation frequencies. If these oscillations were exponentially damped individually, a summation over the damped oscillations would also decay at least exponentially with the smallest decay rate contained in the ensemble of damped oscillations. Thus we can conclude that, on long time scales $\gtrsim$100 ps, there are oscillatory components in the spin polarization that are not significantly damped due to momentum scattering at the impurities.

H. Non-Markovian effects

The discussion of the spin decay times so far was focused on the results of calculations based on the Markovian equations of motion (16). We now move on to discuss non-Markovian effects in the spin dynamics. In Fig. 2(a), the momentum-scattering-dependence of spin decay times obtained from the quantum kinetic equation (13) are presented together with the Markovian results. It is found that in a wide range of momentum scattering rates the Markovian and quantum kinetic calculations predict very similar spin decay times τ_s^f. Only for large momentum scattering rates a quantitative discrepancy is visible.

To investigate the origin of this discrepancy, the time evolution of the spin polarization is plotted in Fig. 6(a) for a case with larger impurity concentration $x = 10\%$ and therefore large momentum scattering rates $\tau_p^{-1} = 1.12$ ps^{-1}. There, the quantum kinetic result decays much faster than the Markovian result. The reason for this is that the redistribution of carriers in $\mathbf{k}$ space, which is accounted for in the quantum kinetic calculations, is completely absent in the Markovian approach. This redistribution can be seen in the inset of Fig. 6(a), which shows the electron distribution at $t = 0$ and 20 ps for both calculations. It can be seen that the electrons are redistributed to states with on average larger wave vectors, which increases the average spin precession frequency and, in accordance with the analytical DP result (21), reduces the spin decay time.

It is noteworthy that the increase in the average wave vector implies an increase in the average kinetic energy, which seems at first glance to be at odds with the conservation of energy.

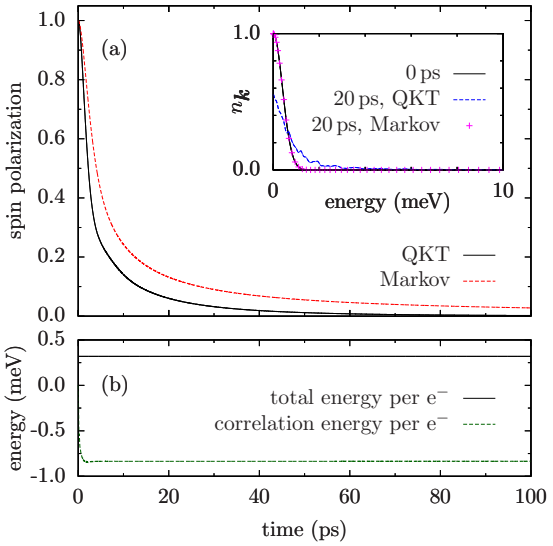

FIG. 6. (a) Comparison of the spin dynamics according to the quantum kinetic theory (QKT) and the Markovian approach for $x = 10\%$, $d = 4$ nm, $\beta_D = 7$ meVnm, $E_c = 0$ meV, and $E_s = 0.4$ meV yielding a momentum scattering rate $\tau_p^{-1} = 1.12$ ps^{-1}. (Inset) The spectral electron distribution for the quantum kinetic and Markovian calculations at $t = 0$ and 20 ps. (b) Dynamics of the average correlation energy as defined in Eq. (26) and the total energy per electron in the quantum kinetic theory.

However, in quantum kinetic calculations that account for correlations, there is a contribution to the total energy resulting from the correlations [65]. Thus the increase of the average single-particle energy is accompanied by a corresponding build-up of negative carrier-impurity correlation energy. This is visualized in Fig. 6(b), where the average correlation energy per particle, defined as

$$\frac{1}{N_e} H_{\mathrm{Imp}}^{\mathrm{cor}} := \frac{JN}{V^2 N_e} \sum_{c\mathbf{k}\mathbf{k}'} \overline{C}_{c\mathbf{k}}^{c\mathbf{k}'} \tag{26}$$

with the total electron number $N_e = \sum_{\mathbf{k}\sigma} C_{\sigma\mathbf{k}}^{\sigma}$, is depicted as a function of time. The total energy per electron, also shown in Fig. 6(b), remains constant. It can be seen that the redistribution of carriers and therefore the build-up of correlation energy is mostly confined to the first few picoseconds of the dynamics.

IV. CONCLUSION

We have studied the spin dynamics in optically excited $Al_xGa_{1-x}As$ quantum wells induced by the interplay of spin precession in $\mathbf{k}$-dependent spin-orbit fields and momentum scattering, i.e., the D'yakonov-Perel' (DP) mechansim [23], using a quantum kinetic theory. Whereas the DP mechanism is usually only described in the strong- and weak-scattering limits, where analytic expressions for the spin relaxation rates can be obtained, we have investigated the dynamics over a wide range of parameters including the limiting cases.

It is found that the time evolution of the spin polarization can be highly nonexponential and the notion of a decay rate for the total spin polarization becomes ambiguous. This can be seen by the fact that two different definitions of the spin decay time, one obtained from a fit of a stretched exponential and

one obtained from the time after which the spin polarization has decayed to $\frac{1}{e}$ of its initial values, show quantitative and qualitative differences in their dependence on the momentum scattering rate.

While it is common to consider only the anisotropic dependence of the spin-orbit fields on the angle of the wave vector as a source of dephasing, we resolve both, the angle and the modulus of the wave vector, allowing us to study situations with nonequilibrium carrier distributions as is the case immediately after the optical excitation with an ultrashort laser pulse. This way, we also include the effects of dispersion-induced isotropic inhomogeneous broadening (DIIB) originating from the dependence of spin-orbit fields on the modulus of the wave vector. Although DIIB has largely been ignored in the literature on the DP mechanism, we find that it strongly influences the spin dynamics after ultrafast optical excitation.

In particular, in the weak-scattering limit, where analytic expressions predict very large spin decay times without DIIB, the dephasing due to DIIB limits the spin decay times even in the absence of momentum scattering. In the strong-scattering limit, the spin decay times are found to be longer than expected from the analytical result since the ensemble of precessing electron spins contains oscillatory components which decay much slower than the average electron spin and, thus, extend the lifetime of the total spin polarization compared to calculations where the spectral electron distribution was assumed to be spectrally sharp and DIIB is suppressed. Some of the oscillatory components are even found to be practically undamped and are responsible for an algebraic decay in the long-time behavior of the total spin polarization that cannot be measured by a spin decay time.

Whereas a linear dependence of the spin decay time on the momentum scattering rate in the strong-scattering limit is usually considered as the hallmark of the DP mechanism, we find that the DIIB introduces an offset leading to an affine linear relationship between spin decay time and momentum scattering rate. Thus DIIB modifies central features of the DP mechansim.

Moreover, we find that DIIB can occur in situations where the spectral electron distribution is narrow if the modulus $\Omega_{\mathbf{k}}$ of the $\mathbf{k}$-dependent precession frequency $\mathbf{\Omega}_{\mathbf{k}}$ depends not only on the modulus of the wave vector but also on its polar angle. This is the case, e.g., if Rashba and Dresselhaus interaction are simultaneously present and of comparable strength. These findings show that DIIB and the effects of broad spectral electron distributions [31], which so far are seldom discussed in the analysis of ultrafast optical experiments dealing with DP-type spin decay, can in fact lead to significant deviations from the analytical results in the strong- [23] and weak-scattering limits [29].

Although our discussion was mostly confined to the Markovian single-electron picture, we have also presented numerical calculations taking electron-impurity correlations explicitly into account. The non-Markovian calculations predict a faster spin decay compared with the Markovian results. This is traced back to the build-up of electron-impurity correlations with negative correlation energies, which enables a redistribution of electrons to states with larger momentum k. This, in turn, increases the average spin precession frequency and enhances the dephasing.

In many experiments, there are other momentum scattering mechanisms to consider. For example, phonon scattering can become important for elevated temperatures, which gives rise to another momentum scattering channel and, in addition, also influences the spin dynamics via the Elliot-Yafet [24–26] mechanism. Furthermore, for p-doped systems the Bir-Aronov-Pikus [27] mechanism affects the spin dynamics, as the electron spins interact with hole spins. In n-doped systems, the electron spin dynamics is modified because of the exchange field resulting from the average carrier spins and the electron-electron scattering, which provides an additional momentum scattering mechanism [38,66].

Note that most of our results are based on a Markovian description where the effects of momentum scattering at the impurities can be subsumed into a momentum scattering rate. The resulting spin dynamics does, however, not depend on the origin of the momentum scattering. Thus the same conclusions for the spin dynamics are reached when other mechanisms are responsible for the momentum scattering, as long as the scattering is approximately elastic. For example, phonon scattering gives rise to a dissipation of energy from the electron system and eventually leads to a thermalization of the electron distribution. This can reduce the average kinetic energy, the average wave vector, and therewith the average spin precession frequency as well as the width of the spectral electron distribution. When the phonon-induced redistribution of carriers in $\mathbf{k}$ space is faster than the typical spin decay time (here, $\lesssim$50 ps), the electron-phonon interaction can enhance the spin decay times since, in the strong-scattering limit, the spin decay time is inversely proportional to the square of the average spin precession frequency and, in the weak-scattering limit, the spin dynamics is dominated by inhomogeneous broadening, which is suppressed if the width of the spectral electron distribution is reduced. More investigations will be needed to study quantitatively the spin dynamics in the presence of inelastic momentum scattering.

ACKNOWLEDGMENT

We gratefully acknowledge the financial support of the Deutsche Forschungsgemeinschaft (DFG) through Grant No. AX17/10-1.

[1] I. Žutić, J. Fabian, and S. Das Sarma, Rev. Mod. Phys. **76**, 323 (2004).

[2] S. A. Wolf, D. D. Awschalom, R. A. Buhrman, J. M. Daughton, S. von Molnár, M. L. Roukes, A. Y. Chtchelkanova, and D. M. Treger, Science **294**, 1488 (2001).

[3] T. Dietl, Nat. Mater. **9**, 965 (2010).

[4] H. Ohno, Nat. Mater. **9**, 952 (2010).

[5] D. Awschalom and M. Flatté, Nat. Phys. **3**, 153 (2007).

[6] Y. Ohno, R. Terauchi, T. Adachi, F. Matsukura, and H. Ohno, Phys. Rev. Lett. **83**, 4196 (1999).

[7] S. Datta and B. Das, Appl. Phys. Lett. **56**, 665 (1990).
[8] I. D'Amico and G. Vignale, Phys. Rev. B **62**, 4853 (2000).
[9] J. Fabian, A. Matos-Abiague, C. Ertler, P. Stano, and I. Zutic, Acta Phys. Slov. **57**, 565 (2007).
[10] J. Wunderlich, B. Kaestner, J. Sinova, and T. Jungwirth, Phys. Rev. Lett. **94**, 047204 (2005).
[11] A. T. Hanbicki, O. M. J. van t Erve, R. Magno, G. Kioseoglou, C. H. Li, B. T. Jonker, G. Itskos, R. Mallory, M. Yasar, and A. Petrou, Appl. Phys. Lett. **82**, 4092 (2003).
[12] I. Appelbaum, B. Huang, and D. J. Monsma, Nature (London) **447**, 295 (2007).
[13] S. A. Crooker, M. Furis, X. Lou, C. Adelmann, D. L. Smith, C. J. Palmstrøm, and P. A. Crowell, Science **309**, 2191 (2005).
[14] R. Fiederling, M. Keim, G. Reuscher, W. Ossau, G. Schmidt, A. Waag, and L. W. Molenkamp, Nature (London) **402**, 787 (1999).
[15] Edited by F. Meier and B. P. Zakharchenya, *Optical Orientation*, Modern Problems in Condensed Matter Sciences Vol. 8 (North-Holland Amsterdam, 1984).
[16] J. M. Kikkawa and D. D. Awschalom, Phys. Rev. Lett. **80**, 4313 (1998).
[17] D. Stich, J. Zhou, T. Korn, R. Schulz, D. Schuh, W. Wegscheider, M. W. Wu, and C. Schüller, Phys. Rev. B **76**, 205301 (2007).
[18] M. Kugler, T. Andlauer, T. Korn, A. Wagner, S. Fehringer, R. Schulz, M. Kubová, C. Gerl, D. Schuh, W. Wegscheider, P. Vogl, and C. Schüller, Phys. Rev. B **80**, 035325 (2009).
[19] X. Marie, T. Amand, P. Le Jeune, M. Paillard, P. Renucci, L. E. Golub, V. D. Dymnikov, and E. L. Ivchenko, Phys. Rev. B **60**, 5811 (1999).
[20] S. A. Crooker, D. D. Awschalom, J. J. Baumberg, F. Flack, and N. Samarth, Phys. Rev. B **56**, 7574 (1997).
[21] J. Schliemann, J. C. Egues, and D. Loss, Phys. Rev. Lett. **90**, 146801 (2003).
[22] M. W. Wu, J. H. Jiang, and M. Q. Weng, Phys. Rep. **493**, 61 (2010).
[23] M. I. D'yakonov and V. I. Perel', Zh. Eksp. Teor. Fiz. **60**, 1954 (1971) [Sov. Phys. JETP **33**, 1053 (1971)].
[24] Y. Yafet, Solid State Phys. **14**, 1 (1963).
[25] R. J. Elliott, Phys. Rev. **96**, 266 (1954).
[26] A. Baral, S. Vollmar, S. Kaltenborn, and H. C. Schneider, New J. Phys. **18**, 023012 (2016).
[27] G. L. Bir, A. G. Aronov, and G. E. Pikus, Zh. Eksp. Teor. Fiz. **69**, 1382 (1975) [JETP **42**, 705 (1975)].
[28] J. Zhou and M. W. Wu, Phys. Rev. B **77**, 075318 (2008).
[29] V. N. Gridnev, J. Exp. Theor. Phys. Lett. **74**, 380 (2001).
[30] M. Wu and C. Ning, Phys. Status Solidi B **222**, 523 (2000).
[31] M. Wu and C. Ning, Eur. Phys. J. B **18**, 373 (2000).
[32] G. Astakhov, V. Kosobukin, V. Kochereshko, D. Yakovlev, W. Ossau, G. Landwehr, T. Wojtowicz, G. Karczewski, and J. Kossut, Eur. Phys. J. B **24**, 7 (2001).
[33] C. Lü, J. L. Cheng, and M. W. Wu, Phys. Rev. B **73**, 125314 (2006).
[34] W. J. H. Leyland, R. T. Harley, M. Henini, A. J. Shields, I. Farrer, and D. A. Ritchie, Phys. Rev. B **76**, 195305 (2007).
[35] M. A. Brand, A. Malinowski, O. Z. Karimov, P. A. Marsden, R. T. Harley, A. J. Shields, D. Sanvitto, D. A. Ritchie, and M. Y. Simmons, Phys. Rev. Lett. **89**, 236601 (2002).
[36] Y. V. Pershin, Phys. Rev. B **75**, 165320 (2007).
[37] J. N. Chazalviel, Phys. Rev. B **11**, 1555 (1975).
[38] J. H. Jiang and M. W. Wu, Phys. Rev. B **79**, 125206 (2009).
[39] J. L. Cheng, M. W. Wu, and J. Fabian, Phys. Rev. Lett. **104**, 016601 (2010).
[40] M. Z. Maialle, Phys. Rev. B **54**, 1967 (1996).
[41] M. W. Wu and H. Metiu, Phys. Rev. B **61**, 2945 (2000).
[42] *Spin Physics in Semiconductors*, edited by M. I. Dyakonov (Springer, Berlin, Heidelberg, 2008).
[43] K. V. Kavokin, Semicond. Sci. Technol. **23**, 114009 (2008).
[44] G. Dresselhaus, Phys. Rev. **100**, 580 (1955).
[45] Y. A. Bychkov and E. I. Rashba, J. Phys. C **17**, 6039 (1984).
[46] R. Winkler, *Spin-Orbit Coupling Effects in Two-Dimensional Electron and Hole Systems*, Springer Tracts in Modern Physics Vol. 191 (Springer, Berlin, 2003).
[47] S. D. Ganichev and L. E. Golub, Phys. Status Solidi B **251**, 1801 (2014).
[48] M. Cygorek, F. Ungar, P. I. Tamborenea, and V. M. Axt, Phys. Rev. B **95**, 045204 (2017).
[49] M. Cygorek, F. Ungar, P. I. Tamborenea, and V. M. Axt, Proc. SPIE **9931**, 993147 (2016).
[50] R. Kubo, J. Phys. Soc. Jpn. **17**, 1100 (1962).
[51] C. Thurn and V. M. Axt, Phys. Rev. B **85**, 165203 (2012).
[52] K. Siantidis, V. M. Axt, and T. Kuhn, Phys. Rev. B **65**, 035303 (2001).
[53] R. Zimmermann, Il Nuovo Cimento D **17**, 1801 (1995).
[54] R. Zimmermann, Phys. Status Solidi B **173**, 129 (1992).
[55] R. Zimmermann and E. Runge, J. Lumin. **60-61**, 320 (1994).
[56] C. Grimaldi, Phys. Rev. B **72**, 075307 (2005).
[57] A similar problem has been described and solved in Ref. [67], where the spin dynamics in diluted magnetic semiconductors in the presence of a **k**-dependent magnetic field was studied.
[58] F. Rossi and T. Kuhn, Rev. Mod. Phys. **74**, 895 (2002).
[59] M. Cygorek and V. M. Axt, Semicond. Sci. Technol. **30**, 085011 (2015).
[60] P. Boross, B. Dóra, A. Kiss, and F. Simon, Sci. Rep. **3**, 3233 (2013).
[61] F. Ungar, M. Cygorek, P. I. Tamborenea, and V. M. Axt, J. Phys.: Conference Series **647**, 012010 (2015).
[62] W. Yi, V. Narayanamurti, H. Lu, M. A. Scarpulla, A. C. Gossard, Y. Huang, J.-H. Ryou, and R. D. Dupuis, Appl. Phys. Lett. **95**, 112102 (2009).
[63] N. S. Averkiev and L. E. Golub, Phys. Rev. B **60**, 15582 (1999).
[64] N. S. Averkiev and L. E. Golub, Semicond. Sci. Technol. **23**, 114002 (2008).
[65] M. Cygorek, P. I. Tamborenea, and V. M. Axt, Phys. Rev. B **93**, 035206 (2016).
[66] M. M. Glazov and E. L. Ivchenko, J. Exp. Theor. Phys. **99**, 1279 (2004).
[67] M. Cygorek, P. I. Tamborenea, and V. M. Axt, Phys. Rev. B **93**, 205201 (2016).